Journal of Hydrology 645 (2024) 132285

Contents lists available at ScienceDirect

Journal of Hydrology

journal homepage: www.elsevier.com/locate/jhydrol

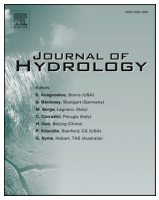

Water and carbon fluxes from a supra-permafrost aquifer to a stream across hydrologic states

Neelarun Mukherjee [a,*], Jingyi Chen [a,b], Bethany T. Neilson [c], George W. Kling [d], M. Bayani Cardenas [a]

[a] Department of Earth and Planetary Sciences, The University of Texas at Austin, USA
[b] Department of Aerospace Engineering and Engineering Mechanics, The University of Texas at Austin, USA
[c] Civil and Environmental Engineering and Utah Water Research Laboratory, Utah State University, USA
[d] Department of Ecology and Evolutionary Biology, University of Michigan, USA

ARTICLE INFO

Keywords:
Hydrology
Groundwater flow
Permafrost
Active-layer
Dissolved organic carbon
Groundwater – surface-water interactions

ABSTRACT

Supra-permafrost aquifers within the active layer are present in the Arctic during summer. Permafrost thawing due to Arctic warming can liberate previously frozen particulate organic matter (POM) in soils to leach into groundwater as dissolved organic carbon (DOC). DOC transport from groundwater to surface water is poorly understood because of the unquantified variability in subsurface properties and hydrological environments. These dynamics must be better characterized because DOC transport to surface waters is critical to predict the long-term fate of recently thawed carbon in permafrost environments. Here, we used distributed Darcy's Law calculations to quantify groundwater and DOC fluxes into Imnavait Creek, Alaska, a representative headwater stream in a continuous permafrost watershed. We developed a statistical ensemble approach to model the parameter variability and range of potential contributions of steady-state groundwater flow to the creek. We quantified the model prediction uncertainty using statistical sampling of in-situ, active-layer soil hydro-stratigraphy (water table, ice table, and soil stratigraphy), high-resolution topography data, and DOC data. Moreover, the predicted groundwater discharge values representing all possible hydrologic conditions towards the end of the thawing season were also considered given the potential variability in saturation. The model predictions were similar to and span most of the observed range of Imnavait Creek streamflow, especially during recession periods, and also during saturation excess overland flow. As the Arctic warms and supra-permafrost aquifers deepen, groundwater flow is expected to increase. This increase is expected to impact stream, river, and lake biogeochemical processes by dissolving and mobilizing more soil constituents in continuous permafrost regions. This study highlights how quantifying the uncertainty of hydro-stratigraphical input parameters helps understand and predict supra-permafrost aquifer dynamics and connectivity to aquatic systems using a simple, but scalable, modeling approach.

1. Introduction

Permafrost occupies around 25 % of the northern hemisphere and 80 % of the Arctic's watersheds (Beer et al., 2020; Zhang et al. 2000a, b), and permafrost soils store twice as much carbon currently present in the atmosphere (Schuur et al., 2015). Higher latitudes where permafrost is present are warming almost four times the rate of the rest of the world (Rantanen et al., 2022; Schaefer et al., 2014). This warming can accelerate permafrost thaw in the Arctic. As a result, previously frozen particulate organic matter can be leached into groundwater as dissolved organic carbon (DOC), which can be respired and released to the atmosphere as carbon dioxide or methane. The release of greenhouse gases leads to additional warming and additional permafrost thaw, creating a positive feedback loop. In permafrost catchments, when the surface soil "active layer" is thawed in summer, the surface water flowing from hillslopes to riparian zones may spend much of its time in the subsurface. That is, even during saturated conditions, the water porpoises between the surface and the subsurface soil (Neilson et al., 2018). Furthermore, in some systems, the contribution of groundwater inflow to surface waters has increased recently due to the thickening of

* Corresponding author.
E-mail address: neelarun@utexas.edu (N. Mukherjee).

https://doi.org/10.1016/j.jhydrol.2024.132285

Available online 9 November 2024

the active layer caused by rising arctic air temperatures (Duan et al., 2017; Nguyen et al., 2022; Qin et al., 2024; Saros et al., 2022; Walvoord and Striegl, 2007).

Previous studies have quantified groundwater flows in continuous permafrost regions using field and numerical modeling methods. For example, field-based active layer groundwater flow studies have used baseflow separation (McNamara et al., 1997; Stieglitz et al., 2003), geochemical methods (Blaen et al., 2014; McNamara et al., 1997; Walvoord and Striegl, 2007), and water balance calculations (Roulet et al., 1993) to quantify groundwater flows. All these studies predicted an increase in groundwater flow and organic matter load to surface waters associated with permafrost degradation. However, most of the arctic permafrost region is hard to access, and in-situ observations of water storage and water flow in the active layer are extremely limited. Therefore, many studies employ numerical models to quantify and predict groundwater contributions to surface waters. Studies based on mechanistic numerical models (Atchley et al., 2015; Frampton et al., 2011; Lamontagne-Hallé et al., 2018; Painter, 2011) account for complex flow physics and groundwater flow dynamics under seasonal variability, but are often parametrized by limited field observations. Simpler models such as TOPMODEL (Stieglitz et al., 1999, 2003) calculated discharge using a topographical index algorithm and integrated fluxes from all pixels in the Digital Elevation Model (DEM) of watersheds. Other models, ARYTHM (Zhang et al. 2000a, b) and TopoFlow (Schramm et al., 2007), also used DEMs to calculate flux from each pixel in the watershed through a grid-based topological geometry to determine the overall water balance of the watershed. An important limitation of these previous DEM-based studies is that they use relatively coarse DEMs (20–25 m pixel spacing), which is likely inadequate for representing the hydrologic dynamics of watersheds with varied ratios of hillslope to valley bottom to riparian zone contributing areas. For example, the riparian-zone, valley bottom, and hillslope transition of some across-valley transects at our study site, the Imnavait Creek watershed, are all within less than 100 m of the creek. Additionally, recent studies that integrated field observations and numerical models suggested that the active layer soil properties such as thaw depth and water table play important roles in quantifying groundwater flux and solute budgets (Evans et al., 2015; O'Connor et al., 2019). However, previous modeling approaches and Investigations have not accounted for the statistical variability in hydrological conditions of the watershed supported by observed properties that dictate flow. Despite prior modeling studies, there are critical gaps in understanding groundwater flow in continuous permafrost watersheds. In many arctic regions, the soil is mainly composed of three distinct layers: the acrotelm (peat containing live and little-decomposed vegetation), the catotelm (older, dead, compacted peat), and mineral soil (Walker, 2000). Of these, acrotelm and catotelm are exceptionally rich in particulate organic matter. The three soil layers have very different hydraulic properties, such as porosity, hydraulic conductivity, and bulk density (e.g., O'Connor et al. (2020b,a)). The seasonal vertical migrations of the water table and ice table within these layers change the net groundwater storage and movement, and thus solute flux, both spatially and temporally (e.g., O'Connor et al. (2019)). To characterize these changes and the dynamics of the active layer requires accounting for the uncertainty associated with the spatial variation in soil hydraulic properties (O'Connor et al., 2020b,a) as well as the spatial and temporal variation in water table and ice table depths (Chen et al., 2020; O'Connor et al., 2019).

This study addresses the question – how much water and dissolved organic matter flux originates from groundwater in supra-permafrost aquifers that contribute to surface waters? The question is addressed using an observation-based, steady-state groundwater flow model that accounts for the statistical variability of field observations. Taking advantage of extensive data from previous field studies (e.g., O'Connor et al. (2020b,a)), we quantified soil stratigraphy and transmissivity and improved the characterization of soil property variation within a steady-state groundwater flow model focused on near-stream head gradients. The groundwater flow estimates were then used to determine the associated DOC loads from land to Imnavait Creek, located in the Toolik Lake area of the North Slope of Alaska.

2. Methods

We apply Darcy's Law to estimate the distribution of riparian-zone groundwater discharge into a creek. More specifically, we use very high-resolution DEMs (20 cm horizontal resolution) next to the channel to determine topographic gradients that drive potential groundwater flux across the bank from land to water. Our computational approach essentially mimics a field-based estimation of Darcy flux with the placement of a piezometer transect of 20 cm horizontal resolution on the bank along the stream for calculating the gradient perpendicular to the stream.

To capture the groundwater and surface water flow dynamics during thaw seasons (from late spring to fall), we employ an ensemble modeling approach using 8,466,850 realizations (or ensemble members) representing likely steady-state snapshots of the watershed hydrological state. Each ensemble model is generated from random sampling of the distributions of in-situ soil property measurements from O'Connor et al. (2020b,a), which independently simulate the groundwater discharge and DOC flux from different states of the active layer along the riparian zone. The relevant soil stratigraphy, hydraulic, and geochemical data are presented here as Extended Datasets 1–7. The ensemble not only represents the uncertainty associated with the natural variability of soil properties, but also the different possible saturation states (partially to fully saturated active layer) due to the variation in the vertical position of the water table and ice table.

In this section, we first describe the study site (Section 2.1). We then explain the model governing equations (i.e., vertically integrated Darcy's Law, Section 2.2.1), and discuss the influence of varying water table and ice table depth. Following that, we describe the model inputs including post processing of the DEM required for calculating the hydraulic head gradient (Section 2.2.2) and identify the statistics of observations (Section 2.2.3). Then we discuss how we estimate total groundwater discharge at different points along the creek and the effect on DOC flux (Section 2.2.4). Finally, we review available field observations and strategies for validating our modeled discharge (Section 2.3).

2.1. Study site

Imnavait Creek is located ~ 10 km east of the Toolik Field Station in the northern foothills of the Brooks Range, Alaska. It is a beaded stream that drains into the Upper Kuparuk River (Fig. 1B). The 2.2 km^2 area of the upper Imnavait Creek watershed is among the most studied watersheds in the Arctic (Kane et al., 1989; McNamara et al., 1997, 1998, 2008; Merck et al., 2011; Merck and Neilson, 2012; O'Connor et al., 2019, 2020; Page et al., 2013; Schramm et al., 2007; Stuefer and Youcha, 2021). The watershed consists of relatively gentle slopes from hilltop heath tundra down to a valley bottom of wet-sedge tundra. The hillslopes are primarily covered with tussock tundra and are bisected by "water tracks". The water tracks begin just below the ridges, are oriented parallel to the slope, and feed directly into a low-gradient riparian zone and function to shorten hydrologic response time to precipitation events (McNamara et al., 1999, 1998). During heavy precipitation events, saturation-excess overland flow is generated within water-tracks that feed surface water to the main channel from the hillslopes.

Throughout the watershed, a similar soil stratigraphy is observed in the supra-permafrost aquifer that has three distinct soil layers: surface acrotelm, mid-depth catotelm, and deeper mineral soil. The thicknesses of these three soil layers vary between hilltop, hillslope, and the valley bottom, which includes the near-stream riparian zone, and the layer thicknesses, are dependent on the type of overlying vegetation

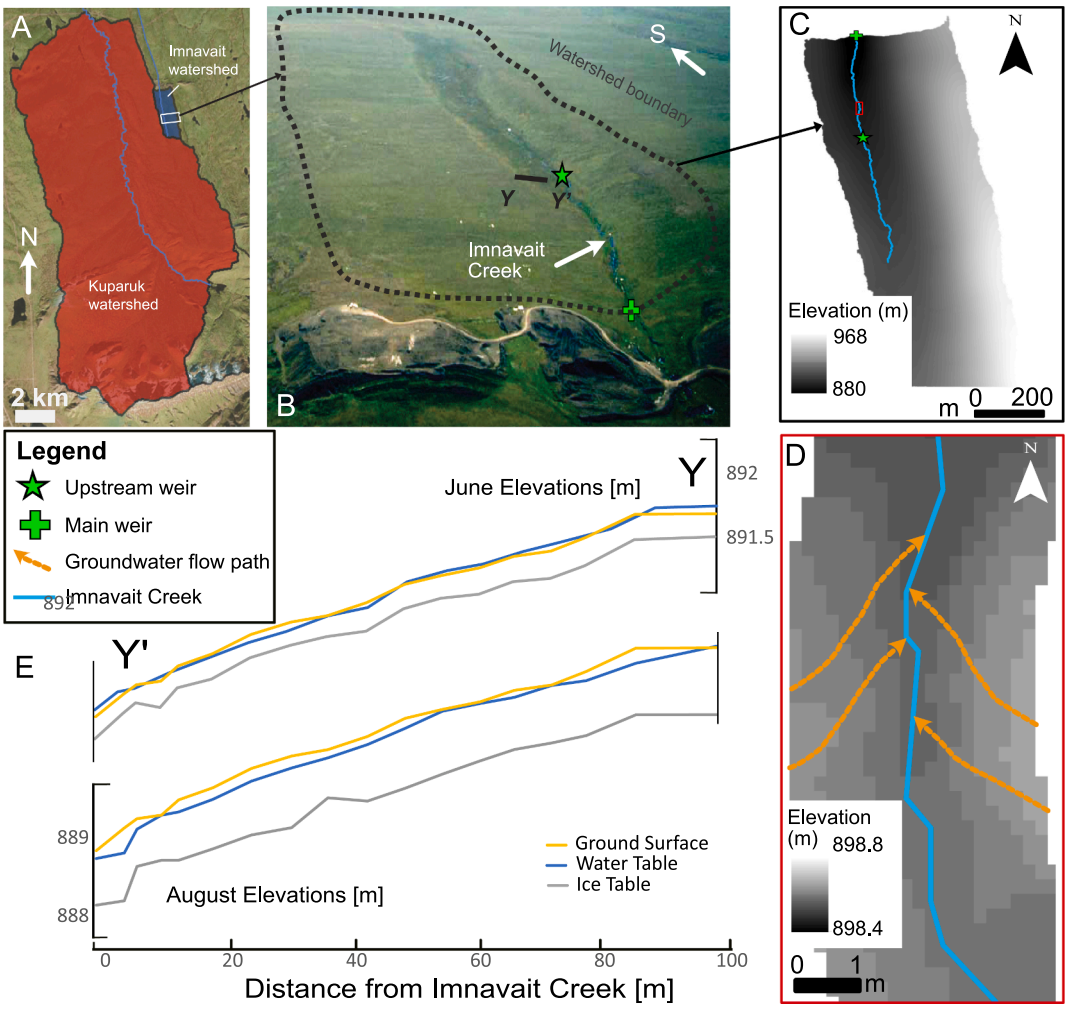

Fig. 1. The study site and depiction of the vertically integrated groundwater flow model based on digital topography. (A) shows the location of Imnavait Creek watershed. (B) shows an oblique air photo of Imnavait Creek. (C) and (D) show the 20-cm resolution digital elevation model of the watershed with example modeled groundwater flow paths. Panel D shows the magnified area enclosed by a red box in panel C. The weir locations used for comparison of total groundwater flow to river discharge in Fig. 3 are marked in (B) and (C). (E) shows the ground surface elevation, groundwater elevation and ice table elevation as measured in June and August 2023 along the transect Y-Y' shown in panel (B). (For interpretation of the references to colour in this figure legend, the reader is referred to the web version of this article.)

(O'Connor et al., 2020). The thaw depth in the study region is representative of tundra located in the northern foothills of the Brooks Range, Alaskan North Slope, where the average end-of-season thaw depth ranges from 39 cm to 72 cm (Circumpolar Active Layer Monitoring Network-CALM, 2023).

Our modeling study domain is the riparian region of the Imnavait Creek watershed from headwaters to the main weir (the Imnavait weir or "Kane weir", 68°37'0.60"N, 149°19'4.30"W) (Stuefer and Youcha, 2021) ("main weir" in Fig. 1B and 1C). This weir is maintained and serviced by the Water and Environmental Research Centre at the University of Alaska at Fairbanks (Extended Dataset 6; Stuefer and Youcha (2021)). Additional discharge data were recorded at an upstream location ("upstream weir" in Fig. 1B and 1C, located at 68°36'38.08"N, 149°18'57.93"W) from a temporary weir used in previous studies (Extended Dataset 7; Neilson et al., 2018; Neilson, 2018). Groundwater samples for dissolved organic carbon (DOC) used in this study were collected from the Imnavait Creek riparian zone since 2010 (Extended Dataset 4; Neilson et al., 2018). The DOC of stream water has been measured for the water from the main weir (Extended Dataset 5; Kling and Dobkowski, 2024).

2.2. Vertically-Integrated groundwater flow modeling

2.2.1. Governing flow equations

Groundwater discharge (Q_{gw} [m^3/s]) at a location of interest is given by the vertically integrated form of Darcy's Law:

$$Q_{gw} = -((K_{eff} \times b) \times w)\nabla h, \quad (1)$$

where K_{eff} is the effective lateral hydraulic conductivity [m/s], b is the saturated thickness (or vertical extent of the aquifer) [m], w is the pixel width [$w = 0.2$ m], and ∇h is the hydraulic head gradient [m/m]. Here, the saturated groundwater flow in an unconfined aquifer is linearized by assuming a known b. The transmissivity (T) is defined as the product of b and saturated hydraulic conductivity (K_{eff}), i.e., $T = K_{eff} \times b$. This assumption is valid for continuous, broad, thin aquifers such as the active layer above continuous permafrost (Fig. 1E).

The groundwater discharge estimates from all stream-adjacent points between the headwaters and the main weir are summed as the total groundwater flow (Q_{gw-tot}[m^3/s]) observed at the weir. The total groundwater flux of DOC as C (carbon) (F_{gw-DOC} in [kg/s]) is then calculated as:

$$F_{gw-DOC} = Q_{gw-tot} \times C_{gw-DOC}, \quad (2)$$

where C_{gw-DOC} [kg/m^3] is the DOC concentration in groundwater. For each ensemble model realization (snapshot), the C_{gw-DOC} is assumed constant throughout the domain.

Effective hydraulic conductivities (K_{eff}) and saturated thicknesses (b) are derived from in-situ field measurements. The in-situ field measurements include depth to water (dtw, in [m]), depth to ice (dti, in [m]), acrotelm thickness (z_{ac}, in [m]), depth to catotelm-mineral soil boundary (dtC, in [m]) and hydraulic conductivities of acrotelm, catotelm and mineral soil (K_{ac}, K_{ct}, K_{mn}, in [m/s]). These in-situ measurements allow us to calculate derived parameters, such as, catotelm thickness (z_{ct}, in [m]), mineral soil thickness (z_{mn}, in [m]) and saturated thickness (b). We note that the relative location of the ice table and water table determines the derived parameters defining a soil column. Hence if a saturated water table is present, i.e., $dtw \leq dti$,

$$b = dti - dtw \quad (3)$$

If the ice table is in mineral soil, i.e., if $dti \geq dtC$,

$$z_{ct} = dtC - z_{ac} \quad (4)$$

$$z_{mn} = dti - dtC \quad (5)$$

if the ice table is in catotelm soil, i.e., $dti > z_{ac}$ and $dti < dtC$,

$$z_{ct} = dti - z_{ac}, \quad (6)$$

and if ice table is in acrotelm layer,

$$z_{ac} = dti \quad (7)$$

To calculate the effective hydraulic conductivity (Fig. 2), consider the first scenario that the ice table is in the mineral soil. If the water table is within the acrotelm, the effective hydraulic conductivity of the saturated layers combined is given by:

$$K_{eff} = \frac{(K_{ac} \times (b - (z_{ct} + z_{mn})) + K_{ct} \times z_{ct} + K_{mn} \times z_{mn})}{b} \quad (8)$$

where K_{ac}, K_{ct}, K_{mn} are the hydraulic conductivities of the acrotelm, catotelm, and mineral soil, respectively, and z_{ac}, z_{ct}, z_{mn} are the respective thicknesses of the three layers. Similarly, when the water table is within the catotelm, the effective hydraulic conductivity is:

$$K_{eff} = \frac{(K_{ct} \times (b - z_{mn}) + K_{mn} \times z_{mn})}{b} \quad (9)$$

and when the water table is in the mineral soil, the effective hydraulic conductivity is:

$$K_{eff} = K_{mn}. \quad (10)$$

Considering the second scenario that the ice table is in the catotelm, if the water table resides in the acrotelm, the effective hydraulic conductivity is given by

$$K_{eff} = \frac{(K_{ct} \times z_{ct} + K_{ac} \times (b - z_{ct}))}{b} \quad (11)$$

If the water table resides in the catotelm, the effective hydraulic conductivity is given by

$$K_{eff} = K_{ct} \quad (12)$$

Considering the third scenario that the ice table is in the acrotelm, the effective hydraulic conductivity is given as

$$K_{eff} = K_{ac} \quad (13)$$

2.2.2. Processing of DEM for vertically integrating modeling

Recent field observations of land surface topography, groundwater table, and ice table both at the start and end of the thawing season suggest that the water table and ice table in the active layer mostly follow the topography (Neilson et al., 2018; O'Connor et al., 2019, 2020) (Fig. 1E). Based on this observation, we can use high-resolution digital elevation models (DEMs) to estimate hydraulic head gradients

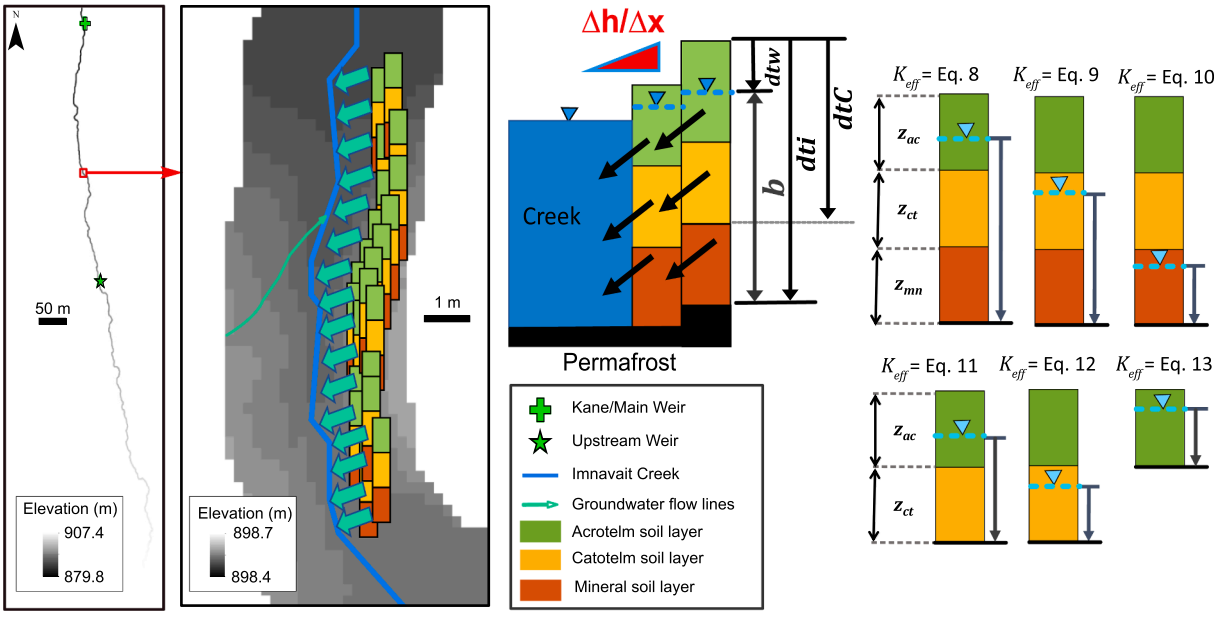

Fig. 2. Model strategy and method. The left panel shows the arrangement of vertical soil layers at each of the cells surrounding Imnavait Creek and how our vertically-integrated model calculates the Q_{gw} for each cell (or DEM pixel). The Q_{gw} of each cell, when integrated along the entirety of Imnavait Creek to a known discharge point such as a weir, gives the Q_{gw-tot} at that location. The middle panel shows how groundwater table in each cell induces flow. The right panel shows how groundwater table varies between each soil layer and how that affects the effective horizontal hydraulic conductivity (Equations (8)–(13)).

(∇h). We used the ArcMAP 'Spatial Analyst' toolbox for calculating the topographic (thus head) gradients at each cell-face along Imnavait Creek, which are held constant for all realizations.

The following standard steps were involved in terrain information processing: (1) filling sinks: here we smoothed the surface of the DEM to create realistic flow paths and reduce numerical errors. In this method, we chose undefined drainage locations (sinks) from the DEM and filled them with elevation values from surrounding cells; (2) flow direction analysis: this step creates a raster by computing flow direction from each cell to its downslope neighbors using the deterministic eight-node, D8 algorithm (Douglas, 1986); (3) flow accumulation analysis: this procedure identified water accumulation in pixels that can delineate the cells in Imnavait Creek that drain to the main weir. Identifying the drainage area allowed us to delineate Imnavait Creek within the DEM.

To calculate topographic head gradients, we used two DEM pixels on both the east and west sides adjacent to Imnavait Creek pixels as the buffer. We found that a minimum of two adjacent pixels aligned perpendicular next to the stream pixels is sufficient to calculate ∇h, and thus the groundwater flux into Imnavait Creek. To confirm this, we increased the buffer width to three and four pixels and used the innermost (streamside) and outermost cells to calculate gradients. This did not produce any notable difference in the hydraulic gradient term in Darcy's Law and thus do not affect the estimated groundwater contributions.

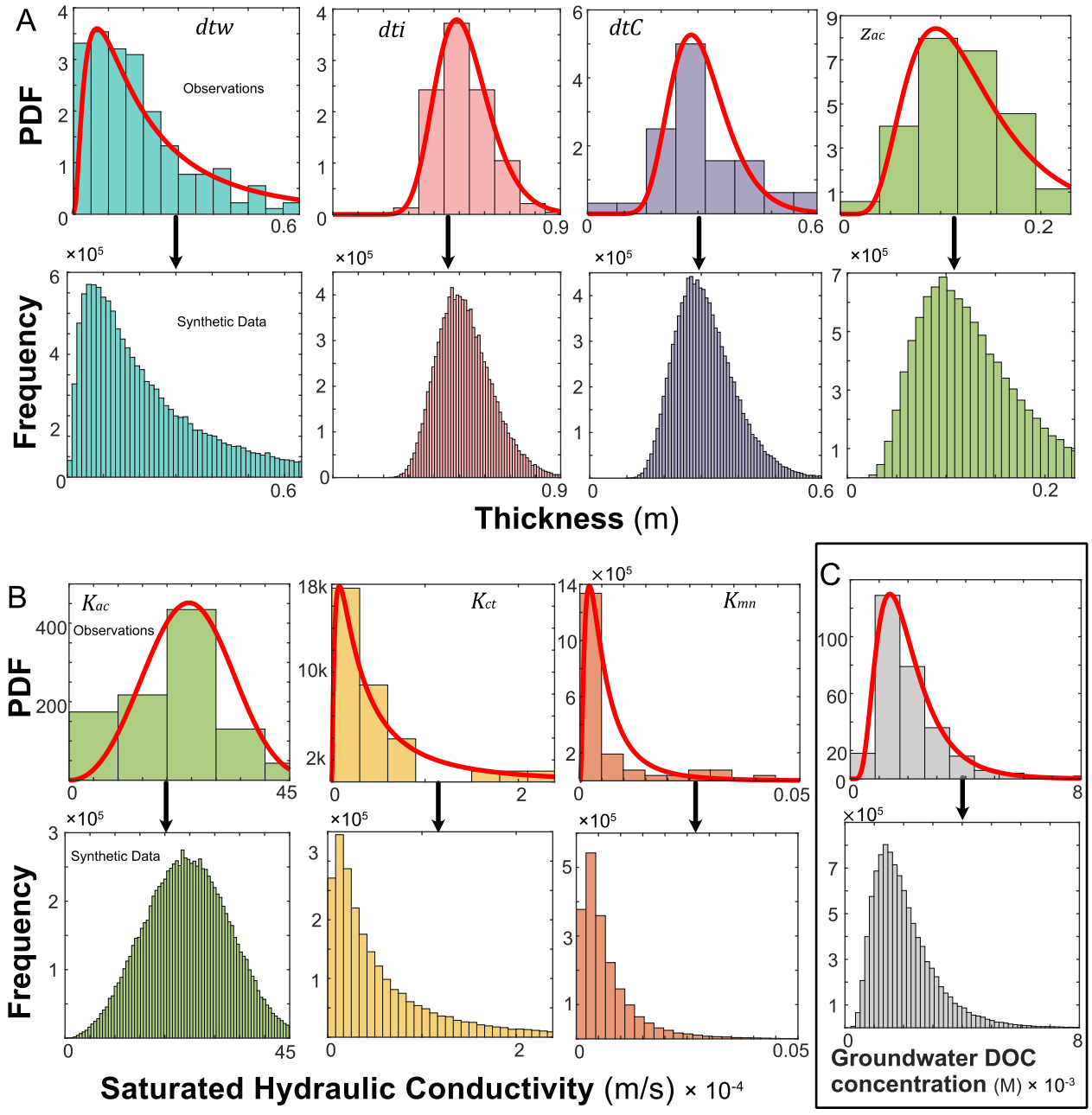

Fig. 3. Input data and results of statistical modeling of parameters for the vertically-integrated groundwater flow model. This figure shows the empirical and modeled (A) field measured thicknesses, depth to water, *dtw*, depth to ice, *dti*, depth to catotelm-mineral soil boundary, *dtC*, acrotelm thickness, z_{ac} (in [m], Extended Dataset 1,3) (B) saturated hydraulic conductivities of each soil layers acrotelm, K_{ac}, catotelm, K_{ct}, mineral soil, K_{mn} (in [m/s], Extended Dataset 2) (C) Groundwater DOC Concentration (in [moles/L], Extended Dataset 4). The first (top) plot shows the observed field parameters on a normalized histogram to which a frequency distribution is fitted and the bottom histogram shows the ensemble parametrization obtained by random sampling from the fitted frequency distribution.

2.2.3. Model input data and their statistics

Our analysis requires field data on aquifer properties for the flow model, chemical data for calculating solute fluxes, and river discharge and chemistry for comparison with the modeled groundwater discharge and solute estimates. Field observations on aquifer properties include soil stratigraphy (depth to acrotelm-catotelm boundary, depth to catotelm-mineral soil boundary), depth to water table, and depth to ice table (i.e., z_{ac}, dtC, dtw, dti). We used *dti* and *dtw* measurements collected from the riparian zone, i.e., from the following measurement grid: broad riparian, near-stream east and near-stream west of O'Connor et al. (2019; see the paper's supplemental information). We also used dti, dtw, and stratum thickness (dtC, z_{ac}) data collected from the riparian zone (from supplemental information of O'Connor et al., 2020). In summary, there are 239 *dti* values, 181 *dtw* values, 45 z_{AC}, and 40 *dtC* values from in-situ field observations. Some of the data from the previously listed studies have been curated further and outliers have been deleted based on physical and observational re-examination of archived field soil samples. All data used in this study are compiled in the Extended Datasets provided with this manuscript.

The distribution (histogram) of each field parameter was fitted with a probability density function (PDF; Fig. 3) by minimizing the misfit between the distribution histogram and fitted PDF. We fitted lognormal PDFs (Eq. (14) to distributions of acrotelm thickness (z_{ac}), depth to catotelm-mineral soil boundary (*dtC*), depth to ice (*dti*), depth to water (*dtw*), and hydraulic conductivities of catotelm and mineral soil (K_{ct}, K_{mn}) as

$$f_X(x) = \frac{1}{x\sigma\sqrt{2\pi}} exp\left(-\frac{(lnx-\mu)^2}{2\sigma^2}\right), \tag{14}$$

where μ is the location parameter and σ is the scale parameter that defines the lognormal distribution. The lognormal mean ($\overline{X}$, expected value) and the standard deviation (*SD*) of the lognormal distribution are given by:

$$\overline{X} = exp\left(\mu + \frac{\sigma^2}{2}\right), \tag{15}$$

$$SD = exp\left(\mu + \frac{\sigma^2}{2}\right)\sqrt{exp(\sigma^2)-1} \tag{16}$$

We fitted a Weibull PDF to the distribution of the hydraulic conductivity of acrotelm (K_{ac})

$$f_X(x) = \begin{cases} \frac{b}{a}\left(\frac{x}{a}\right)^{b-1} \exp\left(-\frac{x}{a}\right)^b, & if x \geq 0 \\ 0, if x < 0 \end{cases} \tag{17}$$

where *a* is the scale parameter and *b* is the shape parameter that defines the Weibull PDF. The Weibull mean ($\overline{X}$, expected value) and the standard deviation (*SD*) are given as:

$$\overline{X} = a\Gamma\left(1+\frac{1}{b}\right) \tag{18}$$

$$SD = a\sqrt{\Gamma\left(1+\frac{2}{b}\right) - \left(\Gamma\left(1+\frac{1}{b}\right)\right)^2} \tag{19}$$

Parameters for all the fitted PDFs to input observations are listed in Table 1.

Next, we draw 10,000,000 random samples from each fitted PDF (Fig. 3A and 3B), which generated 8,466,850 physically possible soil columns. We first defined a soil column by assigning $z_{ac}, z_{ct}, z_{mn}, b$ from the distribution of z_{ac}, dtC, dti, dtw following Eqs. (3)–(7) and including the vertical position of the ice table and water table. Eqs. (8)–(13) determine K_{eff} for each of these 8,466,850 soil column possibilities (Fig. 4). This way we ensure that all generated values of K_{eff} are physically possible in our realizations. A total of 1,533,150 random draws generated nonsensical soil columns based on Eqs. (3)–(13), resulting in the final count of 8,466,850 ensemble members. Specifically, Eqs. (3)–(6) cannot result in numbers $\leq$0. For each ensemble member (Fig. 4), the selected buffer nodes were then assigned randomly-generated soil-column constraints for saturated thickness (*b*) and effective saturated hydraulic conductivity (K_{eff}), hence transmissivity (*T*). Finally, all stream-adjacent cells are assigned the same transmissivity for each realization; where each member is homogeneous in terms of *T*.

2.2.4. Estimation of total groundwater discharge and organic matter flux.

The preprocessed watershed DEM provided the information for the head gradient (∇h) (as discussed in Section 2.2.2). The ∇h and K_{eff} information (Fig. 4A-C) along with 8,466,850 derived values of *b* (Fig. 4D) were used to calculate the flux for each cell on the banks of Imnavait Creek following Eq. (1) (Fig. 2). The integration of flux values at all the pixels along the length of Imnavait Creek until the main weir gives the value of total flux (Q_{gw-tot}) for a single set of input parameters or ensemble realization. Thus, for the ensemble results, we generated flux values at the main weir.

The solute input from groundwater into Imnavait Creek is the product of solute concentration (DOC) and the modeled Q_{gw-tot}(Eq. (2). We have 294 values of groundwater DOC concentrations from the riparian zone. We followed a similar statistical approach of randomly generating 8,466,850 values of groundwater DOC concentration from their lognormal PDF (Eq. (14) (Fig. 3C); the groundwater DOC distribution hasμ = -6.33, σ=0.51, $\overline{X}$=2.0 × 10^{-3} M, and*SD* = 1.1 × 10^{-3} M. A single randomly selected groundwater DOC concentration was assigned to all the river-adjacent cells for each realization. The product of 8,466,850 DOC concentrations and the groundwater fluxes following Eq. (2) provides the modeled groundwater DOC flux ensemble at the main weir. Similarly, the product of mean in-situ DOC concentration of Imnavait Creek from the main weir (Extended Dataset #5) with the river discharge (main weir hydrograph, Stuefer and Youcha (2021)), gives the time series of mean riverine DOC flux. The calculations of solute fluxes were compared from the groundwater flux model estimations and the solute flux observations from the main weir.

Table 1
Statistical distribution parameters for hydraulic conductivities for acrotelm, catotelm, and mineral soil and field measured depths to acrotelm-catotelm boundary (or thickness of acrotelm), catotelm-mineral soil boundary, depth to water table and depth to ice table. The depth data and hydraulic conductivity for catotelm and mineral soil are lognormally distributed, and hydraulic conductivity for acrotelm follows a Weibull distribution. Hence, the corresponding statistical parameters are (μ and σ), lognormal mean ($\overline{X}$), and standard deviation (SD), for the lognormal data, and *a* and *b* parameters for the Weibull distribution. The corresponding extended dataset is included as an Excel Spreadsheet: "ExtendedDatasets_JOH_MukherjeeEtal.xlsx" in Tab 'Dataset 1, 2, 3'.

Statistical parameter	K_{ac}	K_{ct}	K_{mn}	z_{ac}	*dtC*	*dti*	*dtw*
μ(or *a*)	0.00275	−10.15	−14.55	−2.15	−1.20	−0.67	−1.70
σ(or *b*)	3.2	1.25	0.89	0.45	0.26	0.21	1.00
$\overline{X}$(m/s or m)	2.5 × 10^{-3}	8.5 × 10^{-5}	7.1 × 10^{-7}	1.3 × 10^{-1}	3.1 × 10^{-1}	5.2 × 10^{-1}	3.0 × 10^{-1}
SD(m/s or m)	8.4 × 10^{-4}	1.7 × 10^{-4}	7.8 × 10^{-7}	6.0 × 10^{-2}	8.2 × 10^{-2}	1.1 × 10^{-1}	3.9 × 10^{-1}

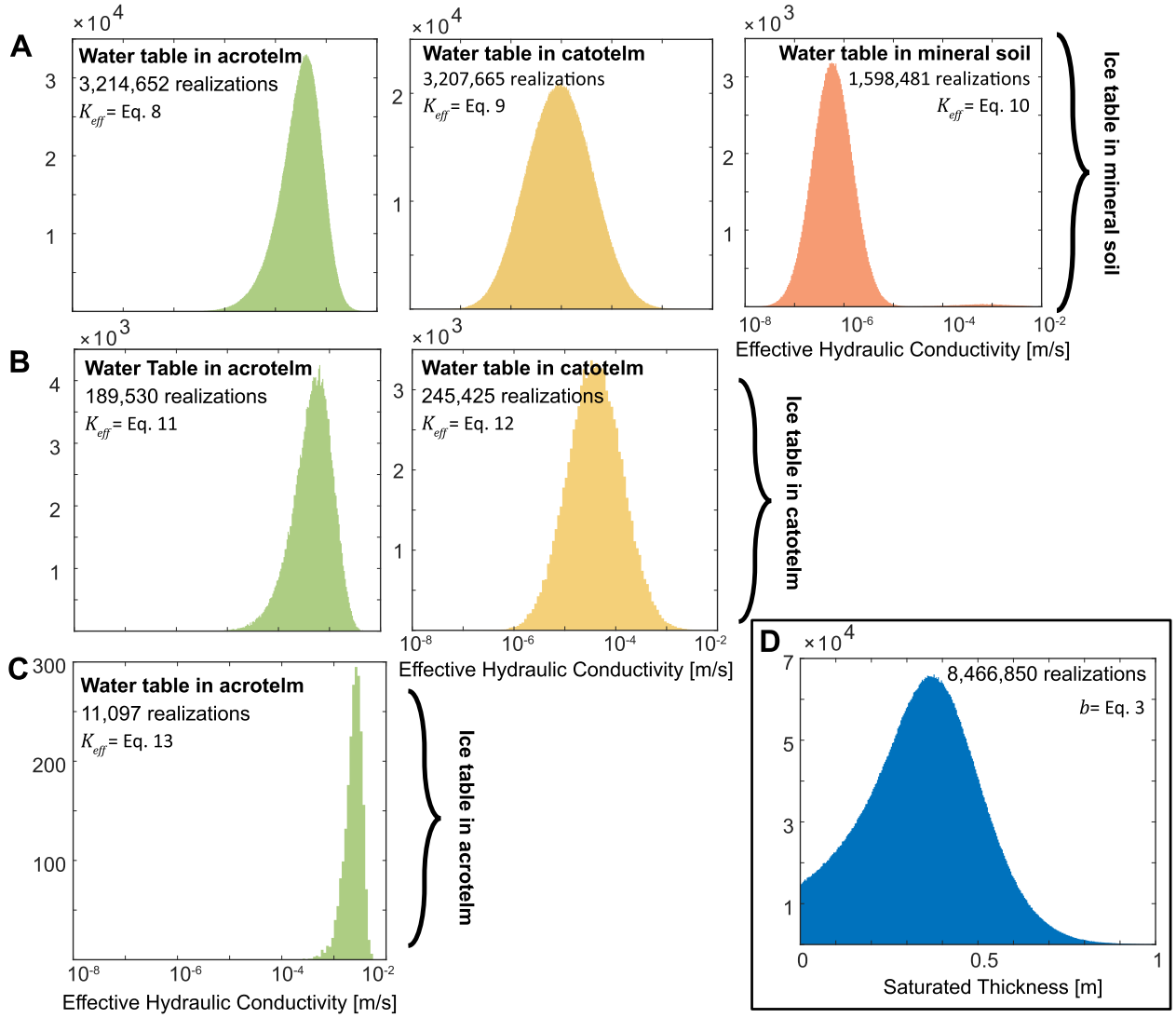

Fig. 4. Total number of realizations of effective hydraulic conductivity (K_{eff}, in [m/s]) for different hydro-stratigraphical snapshots possible from random sampling of primary input variables based on equations (3)–(13). The total number of realizations in each scenario are mentioned in each of the plots. Panel A shows all realizations of effective hydraulic conductivities when the ice table is in mineral soil and water table is in acrotelm, catotelm and mineral soil respectively (from left to right). Panel B shows all possibilities when ice table is in catotelm, and the water table is in acrotelm and catotelm respectively (from left to right). Panel C shows all realizations when the ice table is located in acrotelm, and water table is in acrotelm. Panel D shows the distribution of all physically possible realizations of saturated thicknesses (b, in [m]) from random sampling of depth to water (dtw, in [m]) and depth to ice (dti, in [m]).

2.3. Assessment of modeled groundwater fluxes

We compared the model estimates with field measured variability of river discharge using hydrographs. The model estimates were compared with long-term records of stream discharge and DOC load to determine the relative importance of groundwater in Imnavait Creek's water budget during the thaw season (late spring to early autumn). The hydrograph data cover a variety of scenarios from dry to wet conditions. The model does not capture temporal variations in stream discharge because time variable external forcings were not considered. Therefore, we combined multiple year stream discharge observations for comparison with model estimated discharges and DOC flux. We compared the combined multi-year dataset, and then compared the distribution of observed discharge from years 2006, 2014, 2016 and 2017 to the model-predicted discharge. The predicted discharge simply identifies the possible range of total groundwater discharge using steady-state snapshots. Thus, a point-to-point validation with individual hydrographs is not possible in this study because our model does not explicitly represent time variable responses.

3. Results, Discussion, and Concluding Remarks

3.1. Model input data analysis

The primary model input parameters include dti, dtw, z_{ac}, dtC, and hydraulic conductivities of the soil layers, K_{ac}, K_{ct}, K_{mn}. As noted previously, the K distributions for catotelm and mineral soil follow a lognormal distribution and for acrotelm follow a Weibull distribution (Fig. 3B). The respective distribution mean (expected) value ($\overline{X}$) for K_{ac}, K_{ct}, and K_{mn} are 2.5×10^{-3} (m/s), 8.54×10^{-5} (m/s), and 7.13×10^{-7} (m/s), respectively (Table 1).

The vertical location of the saturated layer in a soil column determines the magnitude of K_{eff} because hydraulic conductivity drastically decreases with depth. If Eq. (3) is valid, i.e., a saturated layer is present, and both the water table and ice table are close to the surface, i.e., the saturated thickness is in the acrotelm, K_{eff} is maximized (following Eq. (13), Figs. 2 and 4). K_{eff} is minimized when the saturated thickness lies in mineral soil (following Eq. (10), Figs. 2 and 4). Along with K_{eff}, the magnitude of saturated thickness, b, also contributes to the

overall magnitude of transmissivity, T. When b is large and is in a thick acrotelm, z_{ac}, the resulting values of T are very large. Oppositely, when b is small and located in mineral soil with very low hydraulic conductivity, the values of T are extremely low. Multiplication of tail-values of highly skewed distributions of b and K_{eff} data (Fig. 4) extends the range of the distribution arising from their combination (Fig. 5).

3.2. Results

The modeled range of groundwater baseflow for the portions of Imnavait Creek analyzed covers a large percentage of the overall range of river discharge observed throughout the summer months (Fig. 5), excluding the freshet. This shows that there can be a substantial groundwater contribution to overall river flow during this time span. Here, we compared the modeling results with the hydrographs recorded from July 1st to September 1st of the years 2006, 2014, 2016, and 2017 for the main weir (Fig. 5A). The range of discharge at the main weir was 0.01 to 310.3 L/s in 2017, spanning four to five orders of magnitude. The 2014 hydrograph shows a continuous recession from 544.5 L/s to 0.02 L/s from August 2nd to August 12th, with continuous baseflow due to the lack of any substantial precipitation events. The 2006 hydrograph also shows continuous recession events from 291 L/s to 3.80 L/s from

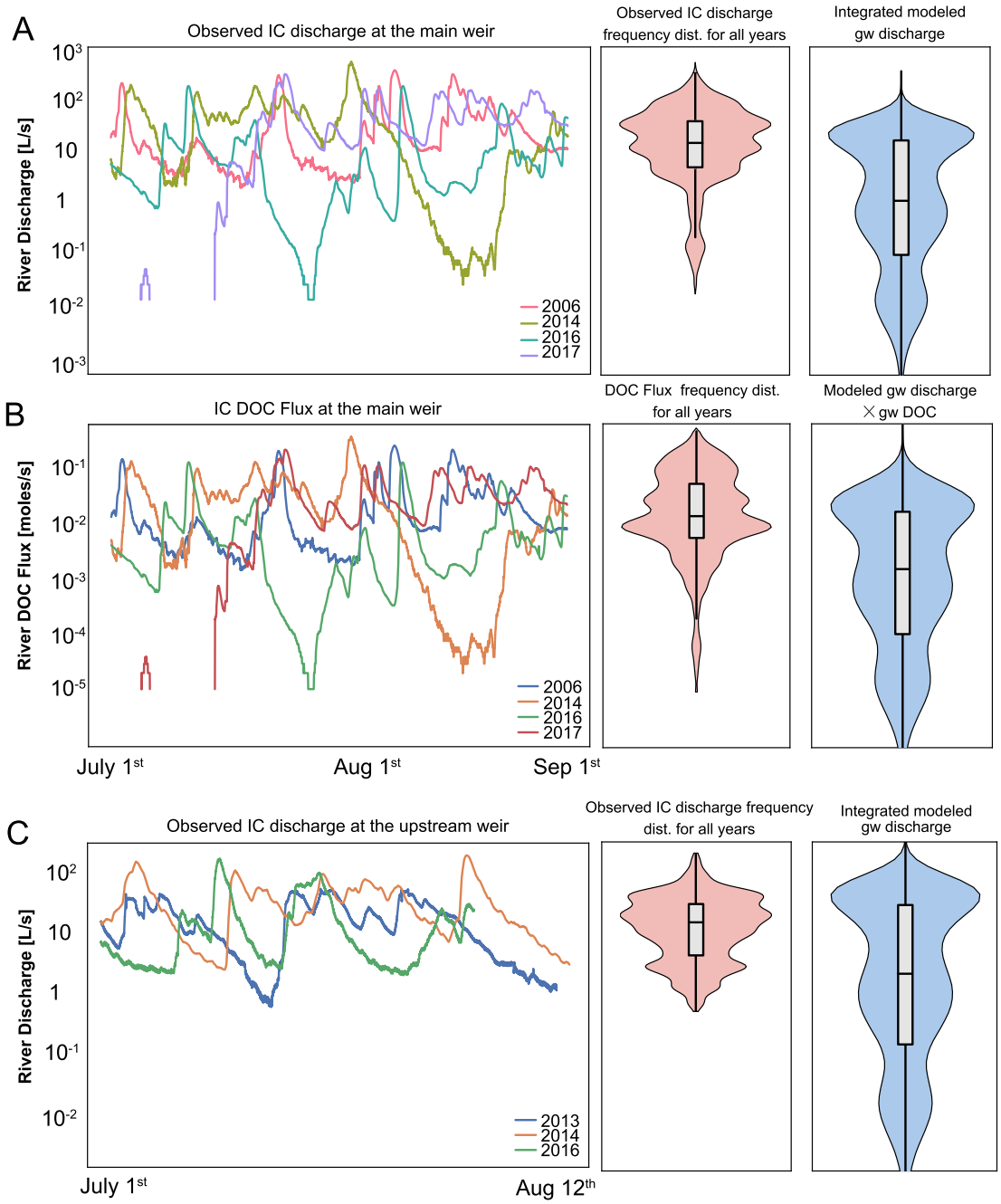

Fig. 5. Panels A and B show the comparison of observed discharge time series (top left), the combined distribution for all years (top center) and modeled groundwater flow (top right), the observation-calculated instream dissolved organic carbon (DOC) flux time series (middle left), the combined distribution (middle center), and the model-calculated groundwater DOC flux for the main weir (see location in Fig. 1C) (middle right) for the years 2006, 2014, 2016, 2017. Panel C shows the comparison of observed discharge, combined statistical distribution for all years, and modeled groundwater flow for another location upstream along the Imnavait Creek (see location of upstream weir in Fig. 1C) for the years 2013, 2014 and 2016. The corresponding boxplots showing the quartiles (Q1, Q2 or median, Q3) are illustrated inside the violin-plots.

July 23rd to July 26th when the flow is near to 100 % baseflow. The 2016 hydrograph also shows continuous recession from 176 L/s on August 9th to 1.18 L/s on August 15th. Thus all 4 years capture peak flow and minimum baseflow during the summer.

The observed discharge ranges for the years 2006, 2014, 2016, 2017 and all years combined, as well as ensemble model results (Table 2), show that in total, 74.6 % of the model ensemble results fall within the observed main weir discharge range. The interquartile discharge range for the groundwater model ensemble almost matches completely with the interquartile discharge range recorded in 2016 at the main weir (Table 2). The peak summer flow conditions, when significant saturation excess overland flow occurs, for all four years, were larger than the third quartile of the groundwater flow model ensemble. Some of these high flow events, especially in 2014 and 2016, receded to flow rates below the ensemble median. The ensemble model third quartile corresponds closely to the median of the observed multiyear discharge recorded at the main weir (Table 2). That is, the ensemble results correspond more with the lower flow (baseflow) regimes (Fig. 5A) of the discharge.

We also compared the modeled groundwater flows and streamflow in Imnavait Creek at an upstream weir location (Fig. 1C). The full range of stream discharge at this upstream weir falls within the range of ensemble model discharge (Table 2, Fig. 5C). Discharge for 58.5 % of the model ensemble overlaps with the range of the combined upstream weir discharge measured for the years 2013, 2014 and 2016. The statistical distribution resulting from combined hydrographs of all three years has the interquartile range nearly overlapping with the median and third quartile of the ensemble model (Table 2, Fig. 5C). For this upstream location, much larger groundwater flows that far exceed the peak flows were also modeled, similar to what was modeled at the main weir. The potential explanations for the results of the comparisons at the main weir and the upstream weir are discussed below.

The main weir hydrograph observations show higher streamflow magnitudes than the ensemble model groundwater inflow predictions. One explanation for this is contribution from overland flow and direct precipitation. This contribution can be accounted for from water tracks located within the watershed on both sides of Imnavait Creek. The water tracks, owing to their lower topography compared to the surrounding land, may intermittently act as tributaries introducing overland flow during and after precipitation from the hillslopes. It is unclear why does not occur at the upstream weir. The ensemble model for the upstream weir location, like that at the main weir, predicts more low flows compared to observations, but its range fully overlaps with the observed streamflow, unlike the main weir. We surmise that this observation can also be explained by the hydrogeomorphic nature of the water tracks. The headwater region is broad and flat where there are anastomosing water tracks and small channels, whereas closer towards the main weir, the hillslopes and riparian zones have a persistently steeper gradient towards the channel, where almost straight water tracks are present. This is somewhat visible in Fig. 1B (look upstream or south of the upstream weir indicated by the green star). As the headwater region is broader and flatter (lower gradient), the diffused and anastomosing water track system in this region may not contribute as much overland flow into the stream compared to steep (high gradient) water tracks located on hillslopes closer to the main weir. This would make the overland flow contribution to the main weir relatively large in comparison to the overland flow contribution to the upstream weir. Moreover, the upstream weir, unlike the main weir, was a temporary installation. This means that the upstream weir design likely did not fully capture the highest flow periods.

In our mass flux calculations, DOC was represented as C (atomic weight of 12.01 g/mol). The uncertainty of stream DOC flux was considered by implementing Eq. (2) for the model with the standard deviation in the measured stream DOC. The overall range of the ensemble model covers the overall ranges of the recorded riverine DOC flux for the years 2006, 2014, 2016, and 2017 (Table 2). The 2014 late summer (beginning August) and 2016 mid-summer (~July) was extremely dry, which resulted in only groundwater feeding the creek; the model ensemble also included such a situation. The median observed DOC flux values combined for years 2006, 2014, 2016 and 2017 align with the third quartile of the model ensemble DOC flux at the main weir (Fig. 5B, Table 2). Also note that observed stream DOC values (Kling and Dobkowski, 2024) include saturation excess overland flow that also contributes to DOC flux (Neilson et al., 2018).

Table 2
Statistics (1st and 3rd quartiles, median or 2nd quartile, minimum and maximum values) of the results of the model ensemble and hydrograph observations for the main weir, upstream weir, and DOC flux at the main weir.

	Q1	Median	Q3	Min	Max
Main weir flow [L/s]					
Modeled groundwater discharge	0.1	1.1	11.26	<0.01	424.38
Observed flow (all years)	4.86	17.1	49.7	0.01	544.5
2006	3.90	8.01	20.7	1.7	367.7
2014	13.9	41.4	73.0	1.1	544.5
2016	0.7	2.94	11.39	0.01	180.07
2017	9.83	20.88	44.7	0.01	310.34
Upstream weir flow [L/s]					
Modeled gw discharge	0.35	3.63	37.06	<0.01	918.74
Observed flow (all years)	4.42	13.99	29.86	0.56	189.99
2013	4.18	12.65	26.20	0.56	52.62
2014	12.18	23.27	51.12	2.35	189.99
2016	2.92	6.84	17.77	1.90	168.64
Main weir DOC Flux [g C/s]					
Modeled groundwater discharge	<0.01	0.02	0.22	<0.01	24.12
Observed flow (all years)	0.09	0.25	0.91	<0.01	7.12
2006	0.07	0.15	0.49	0.02	4.81
2014	0.04	0.25	0.72	<0.01	7.12
2016	0.02	0.05	0.14	<0.01	2.35
2017	0.20	0.44	1.01	<0.01	4.06

3.3. Comparison with previous modeling studies

Earlier research employed various approaches and models to understand groundwater-surface water exchange processes and nutrient transport in permafrost watersheds in the Arctic. Here, we compare our approach to some previous watershed-scale flow modeling studies at our site or similar sites. Similar to our approach, many of the previous hydrological models such as TOPMODEL (Stieglitz et al., 1999, 2003), ARHYTHM (Zhang et al. 2000a, b), and TopoFlow (Schramm et al., 2007) share the same goal of reproducing hydrologic outputs from the watershed, but they involve different underlying assumptions on parameters and processes.

The TOPography based hydrological MODEL or TOPMODEL is used to determine the distribution of soil moisture (water table depth) by representing all points in the watershed using a topographical index – the contributing area divided by the tangent of the slope that is taken from a DEM. The assumption in TOPMODEL is that locations within the watershed with similar indices behave similarly and hence store or release water at the same rate. The index is then used in heuristic equations to calculate the flux and accumulation from each point in the watershed; TOPMODEL calculates the discharge from the watershed as the sum of all flux from all pixels. A TOPMODEL implementation for the Imnavait Creek watershed used DEMs with 20-m resolution (e.g., Stieglitz et al., 1999, 2003). Although TOPMODEL provides simplicity and cost-effective calculations with few parameters, it is a generalized approximation that may not be applicable in various locations, such as Imnavait Creek, where spatial heterogeneity influences hydrology and biogeochemical transport. The ARctic HYdrological and THermal Model or ARHYTHM is a spatially distributed hydrologic model representing both surface (overland) and subsurface (groundwater) flow (Zhang et al. 2000a, b). ARHYTHM considers grid-based topological geometry to determine flow direction to ultimately determine flow. TopoFlow

(Schramm et al., 2007) is a newer version of ARHYTHM with the inclusion of topology-based directional flow, i.e., the D8 algorithm (Douglas, 1986) for routing flow. TopoFlow simulations for the Imnavait Creek watershed were able to model time-varying discharge generally well and captured the over-all water balance of the watershed (Schramm et al., 2007). Like the TOPMODEL implementation for the Imnavait Creek watershed (Stieglitz et al., 1999), TopoFlow was implemented using a coarse DEM with 25 m resolution (that corresponded to the simulation grid spacing) and assumed uniform and vertically homogeneous soil layers. TopoFlow-modeled water table elevations captured observed water tables on the few occasions when the water table was at or near the land surface (see Figure 9 in Schramm et al., 2007). However, the assumptions in the model, especially instantaneous infiltration of recharge from the land surface to the water table (bypassing the unsaturated zone), led to poor representation of fluctuations in the water table. Both TOPMODEL and ARHYTHM or TopoFlow implementations at Imnavait Creek show that these modeling approaches can approximate the over-all watershed mass balance. However, these previous studies (Stieglitz et al., 1999; Zhang et al. 2000a, b; Schramm et al., 2007) have not differentiated quantities of surface (overland flow) and subsurface (groundwater flow) discharge from the hillslope-riparian zones to the creek. Neilson et al. (2018) (Supporting Information: method S3, table S2) estimated groundwater flux using a vertically-integrated model, which is the same approach used in this study, but with a 3-m resolution DEM and compared this to weir discharge measurements during a 3-day baseflow period. Their one realization (compared to 8,433,558 here) using average soil properties showed that both modeled groundwater inflow and creek discharge values are within the same order of magnitude. This is expected given the variability of conditions within the watershed.

This study used a large soil sample dataset to generate PDFs of soil hydraulic parameters and saturated thicknesses. These steps are necessary for determining the spectrum of potential groundwater flux into Imnavait Creek. Watersheds across the Arctic share similar topography and vegetation (Nicolsky et al., 2017; Walker, 2000; Walker et al., 2016), and this statistical approach should be able to represent many other arctic watersheds. Modeling the time-specific behavior and hydrologic dynamics explicitly was not the goal of our analysis, but instead we have produced snapshots of the dynamic range of conditions.

Our ensemble modeling approach considered extensive observations and was able to quantify and consider sources of uncertainty in groundwater flow estimates. However, the approach also has limitations that come from the inherent assumptions of the model. The main limiting assumptions are: (1) all groundwater inflow to the stream is due to topography-driven head gradients in the near-stream riparian zone; and (2) there are no reactions occurring at the stream bank and in-stream, at least in terms of our DOC flux calculations and comparisons. Some of the upslope water flows on the surface through a well-defined water-track network through the hillslope-valley bottom-riparian zone corridor, and thus this surface water input is not captured by our model. The areas beneath water tracks are presumably always saturated and have a relatively higher saturated thickness. The physical parameters like thickness of the soil layers, saturated depth, and depth to the ice table are different for the saturated water tracks and the non-water track locations. These site-specific heterogeneities are not explicitly considered in our model, but are captured by the ranges. Nevertheless, our approach might be capturing or representing such situations with model realizations that have deep thaw, shallow water tables, and highly permeable soils, which all produce very high groundwater discharge. Moreover, while water tracks may not be perfectly or explicitly represented, their flow is nonetheless driven by topographic gradients, which does not violate the first limiting assumption noted above. If some areas near the stream have water tables whose gradients are not as steep as that of the topography or are steeper than topography, then these would clearly lead to bias. We have yet to see these situations in the field. Our limited but detailed water table observations such as those in Fig. 1E support our assumption. Still, it is important to acknowledge that high-resolution field observations are rare. Some exceptions to the assumption are plausible, especially flatter water tables that are the result of persistent drainage with no recharge.

Our approach did not consider biogeochemical reactions at the surface water-groundwater interface or within the water column of the stream. While numerous reactions are possible (e.g., Cory et al., (2015) and Merck et al., (2011)), the suite of groundwater DOC concentrations likely represents waters at different stages of equilibrium with the suite of reactions. The statistical approach to groundwater and stream water DOC, which represents all the DOC measurements available, has likely addressed this potential issue. The outcomes of any reactions are encapsulated in the uncertainty.

3.4. Organic carbon fluxes

Nutrient and organic matter are transported through the active layer by groundwater advection. The soil continually leaches DOC to the groundwater as water flows through the active layer and ultimately to the stream. This leaching happens relatively fast and potentially reaches equilibrium over short periods (Judd and Kling, 2002). This equilibrium would represent the balance between production (leaching and plant root exudation of DOC) and consumptive processes, which include both aerobic and anaerobic respiration and abiotic adsorption to mineral complexes (e.g., iron). Thus, the relatively narrow range and uniformly high groundwater DOC reported in previous studies (as presented in Neilson et al., 2018) might be an outcome of this equilibrium. Our finding that groundwater DOC flux matches well with the instream DOC flux provides further mechanistic support and direct evidence for the ideas put forward by previous studies. For example, McNamara et al. (1997) used isotopic compositions of $\delta^{18}O$ in both groundwater and surface waters to show that groundwater contributes around 80 % of the streamflow, even after a storm event. Neilson et al. (2018) showed that surface water is also mostly groundwater-dominated even after a big storm event due to surface–subsurface exchanges throughout the hillslope and riparian zone, and streamflow DOC concentrations are similar to groundwater DOC concentration. Thus, our study further supports that the DOC chemostasis of Imnavait Creek (Neilson et al., 2018) is due to significant quantities of groundwater entering the stream.

3.5. Conclusions

Our statistical and ensemble groundwater flow modeling approach reproduces the variability of the critical processes and parameters, likely including variability in space and time. The multiphysics groundwater flow and transport mechanisms that govern dynamics in continuous-permafrost watersheds like Imnavait Creek are still being studied and have yet to be applied extensively. However, this study used a saturated steady-state groundwater flow equation with detailed field and experimental data-driven input parametrization to model baseflow contribution to streams. The approach showed that the variability in measured field parameters is necessary to describe the full spectrum of groundwater contribution to streams and provide reasonable predictions when compared to observed stream discharge results over more than one year. Ensemble groundwater DOC flux is also highly correlated with measured stream DOC flux in several different years. Thus, the vertically-integrated model with hydrologic and chemical predictions supports the consistent importance of subsurface groundwater flow-driven DOC export to streams.

CRediT authorship contribution statement

Neelarun Mukherjee: Writing – original draft, Visualization, Validation, Software, Methodology, Investigation, Formal analysis, Data curation, Conceptualization. **Jingyi Chen:** Writing – review & editing, Visualization, Validation, Supervision, Resources, Project

administration, Methodology, Funding acquisition, Conceptualization. **Bethany T. Neilson:** Writing – review & editing, Validation, Methodology, Investigation, Funding acquisition, Data curation, Conceptualization. **George W. Kling:** Writing – review & editing, Validation, Resources, Project administration, Investigation, Funding acquisition, Data curation, Conceptualization. **M. Bayani Cardenas:** Writing – review & editing, Visualization, Validation, Supervision, Resources, Project administration, Methodology, Investigation, Funding acquisition, Data curation, Conceptualization.

Declaration of competing interest

The authors declare that they have no known competing financial interests or personal relationships that could have appeared to influence the work reported in this paper.

Acknowledgements

This research was supported by the U.S. Department of Energy (DOE), Office of Science, Office of Biological and Environmental Research (BER), Environmental System Science (ESS) Program (grant DE-SC0024091), NASA (Terrestrial Hydrology Program (80NSSC18K0983), FINESST (80NSSC20K1622)), and with additional support from the U. S. National Science Foundation (ARC-1204220, DEB-1026843, 1637459, 0639805, and 2224743, PLR-1504006, and OPP-1107593, 1936759). The authors thank Michael O'Connor, Yue Wu, Ke Wang, Jason Dobkowski, Randy Fulweber and Toolik Field Station staff for previous data and facilitating our efforts in the field. The Imnavait Creek watershed is part of the hunting grounds and routes of the Nunamiut, Gwich'in, Koyukuk, and Inupiaq people that continue to inhabit and serve as stewards of the land.

Appendix A. Supplementary data

Supplementary data to this article can be found online at https://doi.org/10.1016/j.jhydrol.2024.132285.

Data availability

Except for topography, all the data used in this study are in the "ExtendedDataset.xlsx" file.

References

Atchley, A.L., Painter, S.L., Harp, D.R., Coon, E.T., Wilson, C.J., Liljedahl, A.K., Romanovsky, V.E., 2015. Using field observations to inform thermal hydrology models of permafrost dynamics with ATS (v0.83). Geosci. Model Dev. 8 (9), 2701–2722. https://doi.org/10.5194/gmd-8-2701-2015.

Beer, C., Zimov, N., Olofsson, J., Porada, P., and Zimov, S., 2020. Protection of Permafrost Soils from Thawing by Increasing Herbivore Density. *Scientific Reports 2020 10:1*, *10*(1), 1–10. https://doi.org/10.1038/s41598-020-60938-y.

Blaen, P.J., Hannah, D.M., Brown, L.E., Milner, A.M., 2014. Water source dynamics of high Arctic river basins. Hydrol. Process. 28 (10), 3521–3538. https://doi.org/10.1002/HYP.9891.

Chen, J., Wu, Y., O'Connor, M., Cardenas, M.B., Schaefer, K., Michaelides, R., Kling, G., 2020. Active layer freeze-thaw and water storage dynamics in permafrost environments inferred from InSAR. Remote Sens. Environ. 248. https://doi.org/10.1016/j.rse.2020.112007.

Circumpolar Active Layer Monitoring Network-CALM: Long-Term Observations of the Climate-Active Layer-Permafrost System., 2023. Retreived from https://www2.gwu.edu/~calm/data/north.htm.

Cory, R.M., Harrold, K.H., Neilson, B.T., Kling, G.W., 2015. Controls on dissolved organic matter (DOM) degradation in a headwater stream: the influence of photochemical and hydrological conditions in determining light-limitation or substrate-limitation of photo-degradation. Biogeosciences 12, 6669–6685. https://doi.org/10.5194/bg-12-6669-2015.

Douglas, D.H., 1986. Experiments to locate ridges and channels to create a new type of digital elevation model. Cartographica: the International Journal for Geographic Information and Geovisualization 23 (4), 29–61. https://doi.org/10.3138/D4L1-1525-N578-2578.

Duan, L., Man, X., Kurylyk, B.L., Cai, T., 2017. Increasing winter baseflow in response to permafrost thaw and precipitation regime shifts in northeastern China. Water 9 (1), 25. https://doi.org/10.3390/W9010025.

Evans, S.G., Ge, S., Liang, S., 2015. Analysis of groundwater flow in mountainous, headwater catchments with permafrost. Water Resour. Res. 51 (12), 9564–9576. https://doi.org/10.1002/2015WR017732.

Frampton, A., Painter, S., Lyon, S.W., Destouni, G., 2011. Non-isothermal, three-phase simulations of near-surface flows in a model permafrost system under seasonal variability and climate change. J. Hydrol. 403 (3–4), 352–359. https://doi.org/10.1016/j.jhydrol.2011.04.010.

Judd, K.E., Kling, G.W., 2002. Production and export of dissolved C in arctic tundra mesocosms: the roles of vegetation and water flow. Biogeochemistry 60, 213–234. https://doi.org/10.1023/A:1020371412061.

Kane, D.L., Hinzman, L.D., Benson, C.S., Everett, K.R., 1989. Hydrology of Imnavait Creek, an arctic watershed. Ecography 12 (3), 262–269. https://doi.org/10.1111/J.1600-0587.1989.TB00845.X.

Kling, G. and Dobkowski, J., 2024. Dissolved organic carbon (DOC) in Imnavait Creek, Foothills, Brooks Range, Alaska, 2002-2009. ver 1. Environmental Data Initiative. https://doi.org/10.6073/pasta/057404728eb931f41455c5c5c5ca6652 (Accessed 2024-10-31).

Lamontagne-Hallé, P., McKenzie, J.M., Kurylyk, B.L. and Zipper, S.C., 2018. Changing groundwater discharge dynamics in permafrost regions. *Environmental Research Letters*, *13*(8), p.084017. https://doi.org/ 10.1088/1748-9326/aad404.

McNamara, J.P., Kane, D.L., Hinzman, L.D., 1997. Hydrograph separations in an Arctic watershed using mixing model and graphical techniques. Water Resour. Res. 33 (7), 1707–1719. https://doi.org/10.1029/97WR01033.

McNamara, J.P., Kane, D.L., Hinzman, L.D., 1998. An analysis of streamflow hydrology in the Kuparuk River Basin, Arctic Alaska: a nested watershed approach. J. Hydrol. 206 (1–2), 39–57. https://doi.org/10.1016/S0022-1694(98)00083-3.

McNamara, J.P., Kane, D.L., Hinzman, L.D., 1999. An analysis of an arctic channel network using a digital elevation model. Geomorphology 29 (3–4), 339–353. https://doi.org/10.1016/S0169-555X(99)00017-3.

McNamara, J.P., Kane, D.L., Hobbie, J.E., Kling, G.W., 2008. Hydrologic and biogeochemical controls on the spatial and temporal patterns of nitrogen and phosphorus in the Kuparuk River, arctic Alaska. Hydrological Processes: an International Journal 22 (17), 3294–3309. https://doi.org/10.1002/HYP.6920.

Merck, M.F., Neilson, B.T., Cory, R.M., Kling, G.W., 2011. Variability of in-stream and riparian storage in a beaded arctic stream. Hydrol. Process. 26 (19), 2938–2950. https://doi.org/10.1002/hyp.8323.

Merck, M.F., Neilson, B.T., 2012. Modelling in-pool temperature variability in a beaded arctic stream. Hydrol. Process. 26 (25), 3921–3933. https://doi.org/10.1002/hyp.8419.

Neilson, B.T., Cardenas, M.B., O'Connor, M.T., Rasmussen, M.T., King, T.V., Kling, G.W., 2018. Groundwater Flow and Exchange Across the Land Surface Explain Carbon Export Patterns in Continuous Permafrost Watersheds. Geophys. Res. Lett. 45 (15), 7596–7605. https://doi.org/10.1029/2018GL078140.

Neilson, B.T., 2018. NSF-ARC 1204220: Kuparuk River and Imnavait Creek. HydroShare. http://www.hydroshare.org/resource/713e8be6255d404980a3f67cef7337ee.

Nguyen, H.T., Lee, Y.M., Hong, J.K., Hong, S., Chen, M., Hur, J., 2022. Climate warming-driven changes in the flux of dissolved organic matter and its effects on bacterial communities in the Arctic Ocean: A review. Front. Mar. Sci. https://doi.org/10.3389/fmars.2022.968583.

Nicolsky, D.J., Romanovsky, V.E., Panda, S.K., Marchenko, S.S., Muskett, R.R., 2017. Applicability of the ecosystem type approach to model permafrost dynamics across the Alaska North Slope. J. Geophys. Res. Earth 122 (1), 50–75. https://doi.org/10.1002/2016JF003852.

O'Connor, M.T., Cardenas, M.B., Neilson, B.T., Nicholaides, K.D., Kling, G.W., 2019. Active Layer Groundwater Flow: The Interrelated Effects of Stratigraphy, Thaw, and Topography. Water Resour. Res. 55 (8), 6555–6576. https://doi.org/10.1029/2018WR024636.

O'Connor, M.T., Cardenas, M.B., Kling, G., Chen, J., 2020. Soil stratigraphic data for the Toolik Lake region, North Slope of Alaska 2016–2019. Environmental Data Initiative. https://doi.org/10.6073/pasta/68ab4e6f628909de50409df766e183d7 (Accessed 2023-03-28).

O'Connor, M.T., Cardenas, M.B., Ferencz, S.B., Wu, Y., Neilson, B.T., Chen, J., Kling, G. W., 2020. Empirical models for predicting water and heat flow properties of permafrost soils. Geophys. Res. Lett. 47 (11), e2020GL087646. https://doi.org/10.1029/2020GL087646.

Page, S.E., Kling, G.W., Sander, M., Harrold, K.H., Logan, J.R., McNeill, K., Cory, R.M., 2013. Dark formation of hydroxyl radical in arctic soil and surface waters. Environ. Sci. Tech. 47 (22), 12860–12867. https://doi.org/10.1021/es4033265.

Painter, S.L., 2011. Three-phase numerical model of water migration in partially frozen geological media: Model formulation, validation, and applications. Comput. Geosci. 15 (1), 69–85. https://doi.org/10.1007/s10596-010-9197-z.

Qin, J., Ding, Y., Shi, F., Cui, J., Chang, Y., Han, T., Zhao, Q., 2024. Links between seasonal suprapermafrost groundwater, the hydrothermal change of the active layer, and river runoff in alpine permafrost watersheds. Hydrol. Earth Syst. Sci. 28 (4), 973–987. https://doi.org/10.5194/hess-28-973-2024.

Rantanen, M., Karpechko, A.Y., Lipponen, A., Nordling, K., Hyvärinen, O., Ruosteenoja, K., Vihma, T., Laaksonen, A., 2022. The Arctic has warmed nearly four times faster than the globe since 1979. Commun. Earth Environ. 3 (1), 168. https://doi.org/10.1038/s43247-022-00498-3.

Roulet, N.T., Ash, R., Quinton, W., Moore, T., 1993. Methane flux from drained northern peatlands: effect of a persistent water table lowering on flux. Global Biogeochem. Cycles 7 (4), 749–769. https://doi.org/10.1029/93GB01931.

Saros, J.E., Arp, C.D., Bouchard, F., Comte, J., Couture, R.M., Dean, J.F., Lafrenière, M., MacIntyre, S., McGowan, S., Rautio, M., Prater, C., 2022. Sentinel responses of Arctic freshwater systems to climate: linkages, evidence, and a roadmap for future research. Arct. Sci. 9 (2), 356–392. https://doi.org/10.1139/AS-2022-0021.

Schaefer, K., Lantuit, H., Romanovsky, V.E., Schuur, E.A., Witt, R., 2014. The impact of the permafrost carbon feedback on global climate. Environ. Res. Lett. 9 (8), 085003. https://doi.org/10.1088/1748-9326/9/8/085003.

Schramm, I., Boike, J., Bolton, W.R., Hinzman, L.D., 2007. Application of TopoFlow, a spatially distributed hydrological model, to the Imnavait Creek watershed. Alaska. *Journal of Geophysical Research: Biogeosciences* 112 (G4). https://doi.org/10.1029/2006JG000326.

Schuur, E.A., McGuire, A.D., Schädel, C., Grosse, G., Harden, J.W., Hayes, D.J., Hugelius, G., Koven, C.D., Kuhry, P., Lawrence, D.M., Natali, S.M., 2015. Climate change and the permafrost carbon feedback. Nature 520 (7546), 171–179. https://doi.org/10.1038/nature14338.

Stieglitz, M., Hobbie, J., Giblin, A., Kling, G., 1999. Hydrologic modeling of an arctic tundra watershed: Toward Pan-Arctic predictions. J. Geophys. Res. Atmos. 104 (D22), 27507–27518. https://doi.org/10.1029/1999JD900845.

Stieglitz, M., Shaman, J., McNamara, J., Engel, V., Shanley, J., Kling, G.W., 2003. An approach to understanding hydrologic connectivity on the hillslope and the implications for nutrient transport. Global Biogeochem. Cycles 17 (4). https://doi.org/10.1029/2003gb002041.

Stuefer, S.L., Youcha, E.K., 2021. Hydrology of Imnavait Creek and Kuparuk River in Alaska. University of Alaska Fairbanks, Water and Environmental Research Center https://ine.uaf.edu/werc/imnavait (Accessed July 1, 2021).

Walker, D.A., 2000. Hierarchical subdivision of Arctic tundra based on vegetation response to climate, parent material and topography. Glob. Chang. Biol. 6 (S1), 19–34. https://doi.org/10.1046/J.1365-2486.2000.06010.X.

Walker, D.A., Daniëls, F.J.A., Alsos, I., Bhatt, U.S., Breen, A.L., Buchhorn, M., Bültmann, H., Druckenmiller, L.A., Edwards, M.E., Ehrich, D., Epstein, H.E., 2016. Circumpolar Arctic vegetation: a hierarchic review and roadmap toward an internationally consistent approach to survey, archive and classify tundra plot data. Environ. Res. Lett. 11 (5), 055005. https://doi.org/10.1088/1748-9326/11/5/055005.

Walvoord, M.A., Striegl, R.G., 2007. Increased groundwater to stream discharge from permafrost thawing in the Yukon River basin: Potential impacts on lateral export of carbon and nitrogen. Geophys. Res. Lett. 34 (12). https://doi.org/10.1029/2007GL030216.

Zhang, T., Heginbottom, J.A., Barry, R.G., Brown, J., 2000a. Further statistics on the distribution of permafrost and ground ice in the Northern Hemisphere. Polar Geogr. 24 (2), 126–131. https://doi.org/10.1080/10889370009377692.

Zhang, Z., Kane, D.L., Hinzman, L.D., 2000b. Development and application of a spatially-distributed Arctic hydrological and thermal process model (ARHYTHM). Hydrol. Process. 14 (6), 1017–1044. https://doi.org/10.1002/(SICI)1099-1085(20000430)14:6.